Physicochemical Determinants of Passive Membrane Permeability: Role of Solute Hydrogen-Bonding Potential and Volume

Jay T. Goodwin, Robert A. Conradi, Norman F. H. Ho, and Philip S. Burton*

Drug Absorption and Transport, Pharmaceutical Development, Pharmacia, Kalamazoo, Michigan 49007

Received June 6, 2001

The relationship of solute structure with cellular permeability was probed. Two series of dipeptide mimetics consisting of glycine, alanine, valine, leucine, phenylalanine, and cyclohexylalanine with amino acids in the D-configuration were prepared. Partition coefficients for the peptidemimetics were obtained in the octanol/water (log $P_{octanol/water}$), hydrocarbon/octanol (Δ log P), and heptane/ethylene glycol (log $P_{heptane/glycol}$) systems in order to explore the contributions of solute volume, or surface area, and hydrogen-bond potential to the permeability of the solutes. Permeability coefficients were obtained in Caco-2 cell monolayers as a model of the human intestinal mucosa. The results were interpreted in terms of a partition/diffusion model for solute transport where membrane partitioning into the permeability-limiting membrane microdomain is estimated from the solvent partition coefficients. Neither log $P_{octanol/water}$ nor Δ log P alone correlated with cellular permeability for all the solutes. In contrast, log $P_{heptane/glycol}$ gave a qualitatively better correlation. With regard to solute properties, log $P_{octanol/water}$ is predominantly a measure of solute volume, or surface area, and hydrogen-bond acceptor potential, while Δ log P is principally a measure of hydrogen-bond donor strength. Log $P_{heptane/glycol}$ contains contributions from all these solute properties. The results demonstrate that both hydrogen-bond potential and volume of the solutes contribute to permeability and suggests that the nature of the permeability-limiting microenvironment within the cell depends on the properties of a specific solute. Collectively, these findings support the conclusion that a general model of permeability will require consideration of a number of different solute structural properties.

Introduction

In the absence of significant chemical degradation or metabolism, the rate and extent of absorption of a drug after oral administration is dependent upon the concentration of the drug in the intestinal lumen and permeability of the intestinal mucosa to the drug.[1−3] In many cases, especially with high-dose drugs, the concentration effectively equates with the solubility of the drug in the lumen. Both solubility and permeability are properties dependent upon the structural characteristics of the drug. Clearly, a better understanding of the relationship of solute structure with these properties will be useful in the design of drugs with improved bioavailability.

The relationship of solute structure with permeability depends on the mechanism of permeation. As shown in Figure 1, permeability of a solute from the intestinal lumen to the portal circulation necessitates movement through a number of environments, each of which can be considered a resistance.[4−6] At a minimum, the solute must cross the mucus coat and associated unstirred water layer overlying the continuous epithelial cell monolayer comprising the intestinal epithelium. Transport across the epithelium can be by a transcellular (through the cell) pathway and/or a paracellular (between adjacent epithelial cells) pathway.[7] Furthermore, the transcellular pathway involves crossing the apical plasma membrane, movement through the cytosol, and passage across the basolateral membrane. The paracellular pathway is an aqueous route restricted by the presence of tight junctions between the cells.[8,9] Finally, to gain access to the mesenteric circulation draining the epithelium, the solute must cross the basement membrane underlying the epithelial cells and overlying the lamina propria, through the interstitial space, and across the capillary endothelium. Given that these environments, or potential resistances, have different properties, the influence of solute structure upon each

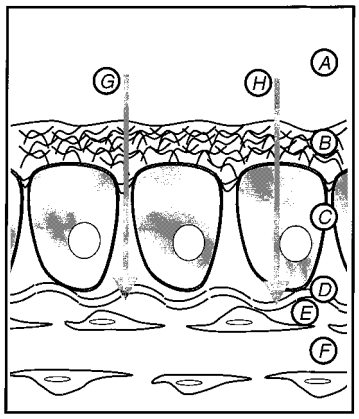

Figure 1. Schematic representation of barriers to and pathways of intestinal permeability: (A) intestinal lumen; (B) mucus; (C) enterocytes; (D) basement membrane; (E) interstitium; (F) capillary; (G) paracellular permeation; and (H) transcellular permeation.

* Address correspondence to this author: Phone 616-833-1322; fax 616-833-2325; e-mail philip.s.burton@am.pnu.com.

10.1021/jm010253i CCC: $20.00
Published on Web 09/25/2001

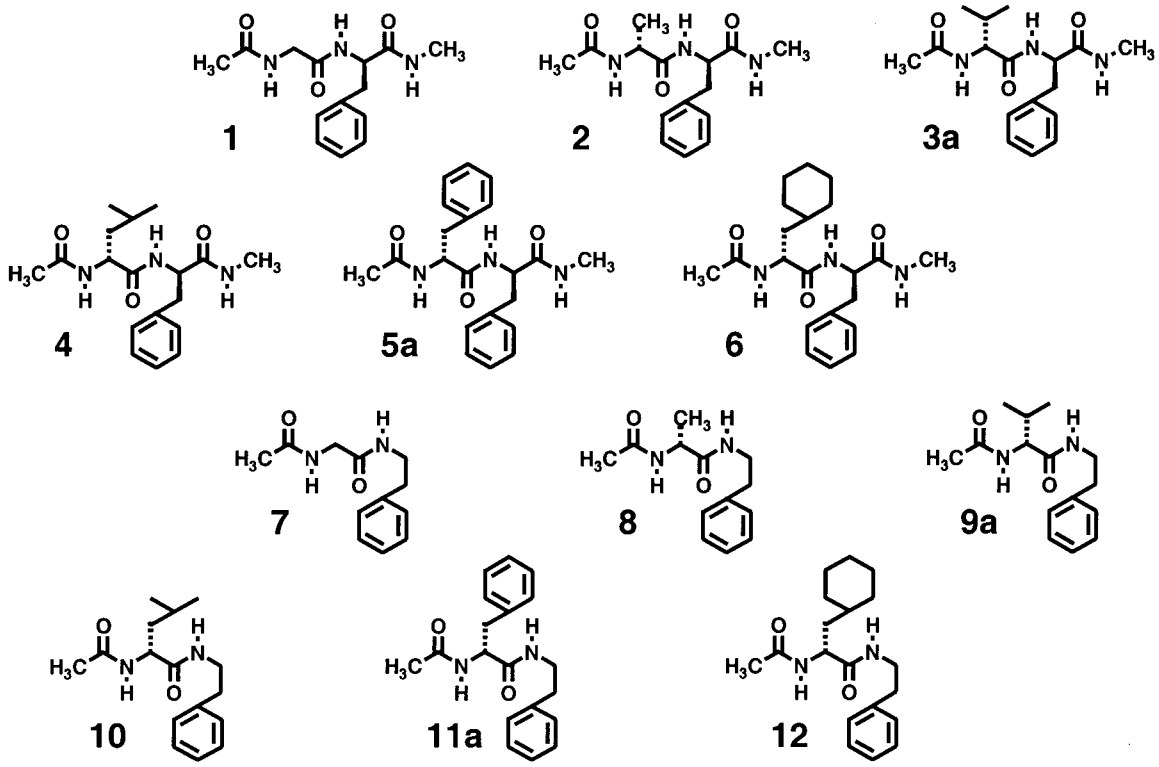

Figure 2. X-phenylalanine dipeptide and *X*-phenethylamide peptidomimetic series, where X = Gly, D-Ala, D-Val, D-Leu, D-Phe, and d-cyclohexylalanine.

resistance will be different, resulting overall in a highly complicated modeling problem.

To simplify this process for modeling purposes, a common strategy has been to collapse all of these steps into a single, homogeneous membrane transport process. This assumes that, for a given series of solutes, one of these steps is the overall permeability-limiting process and the others can be ignored. In some cases, the unstirred aqueous boundary layer resistance and parallel transcellular and paracellular pathways are considered explicitly in exploring structure−transport relationships. In previous work, we have used such a model to examine the role of solute structure in transport of a series of model peptide mimetics across Caco-2 cell monolayers.[10,11] Caco-2 cells are human colon adenocarcinoma cells that form confluent monolayers in culture once seeded onto filter membranes. These monolayers spontaneously differentiate into a polarized, enterocytelike morphology which mimics that of the small intestinal epithelium.[12−16] Using this model we found that the permeability of these peptide mimetics was dependent upon the hydrogen-bonding potential of the solutes. This was estimated from the total number of hydrogen bonds possible or, experimentally, $\Delta \log P$ (obtained from $\log P_{\text{hydrocarbon/water}} - \log P_{\text{octanol/water}}$). Permeability was significantly less correlated with octanol−water partition coefficients, a commonly employed surrogate for predicting oral absorption.[10,11,17] In the present studies, these relationships were further explored by designing two additional series of peptide mimetics (Figure 2) in which hydrogen-bond potential was held constant while octanol−water partition coefficients varied in an incremental fashion.

Table 1. Permeability Data for Compounds **1**−**12**

	p_{eff}			$p_{\text{eff,verapamil}}$						
compound	AP → BL[a]	BL → AP[a]	ratio[b]	AP → BL[a]	BL → AP[a]	ratio[b]	p_{mono}[c]	p_{para}[c]	p_{trans}[c]	log p_{trans}
1	0.17	0.24	1.4	0.14	0.12	0.9	0.14	0.60	0.00	
2	0.24	0.38	1.6	0.25	0.25	1.0	0.25	0.56	0.00	
3a	0.91	1.84	2.0	0.89	0.78	0.9	0.90	0.48	0.42	6.38
4	1.41	2.24	1.6	1.52	1.42	0.9	1.56	0.44	1.12	5.95
5a	2.75	5.19	1.9	2.80	2.64	0.9	2.95	0.37	2.58	5.59
6	7.20	14.5	2.0	8.93	9.02	1.0	10.7	0.36	10.3	4.99
7	21.9	20.6	0.9	22.6	20.8	0.9	38.4	0.77	37.6	4.42
8	24.6	22.9	0.9	25.2	23.5	0.9	46.5	0.71	45.8	4.34
9a	34.5	32.4	0.9	35.1	33.0	0.9	97.0	0.60	96.4	4.02
10	42.6	47.2	1.1	47.4	47.7	1.0	343	0.56	342	3.47
11a	52.0	56.8	1.1	55.1	59.5	1.1				
12	58.3	58.4	1.0	55.5	55.6	1.0				

[a] AP → BL = apical-to-basolateral permeability; BL → AP = basolateral-to-apical permeability. [b] Ratio of BL → AP to AP → BL permeabilities. [c] p_{mono} = monolayer permeability, p_{para} = paracellular permeability, p_{trans} = transcellular permeability; permeabilities are given in units of 10^{-6} centimeters per second. Standard errors in permeabilities are ≤10%, $n \geq 4$, except for compounds **7**, **8**, **9a**, and **10**, where the standard error is ≤30%. The mass balances for all permeabilities determined are 100% (±10%).

Results

The effective, monolayer, and transcellular permeabilities for the X-D-Phe and X-phenethylamide peptide series are given in Table 1. The effective permeability of a given compound is a complex function of aqueous boundary layers and cell monolayer and filter permeabilities, as described in Figure 1. This is represented, analogously to resistances in series, as

$$\frac{1}{p_{\text{eff}}} = \frac{1}{p_{\text{ABL}}^{\text{ap}}} + \frac{1}{p_{\text{mono}}} + \frac{1}{p_{\text{filter}}} + \frac{1}{p_{\text{ABL}}^{\text{bl}}} \qquad (1)$$

where p_{eff} is the effective permeability coefficient for the

solute, p_{ABL}^{ap} and p_{ABL}^{bl} are aqueous boundary layer permeabilities for the apical and basolateral compartments, respectively, p_{filter} is the polycarbonate filter permeability, and p_{mono} is the Caco-2 cell monolayer permeability.[18,19]

In previous studies, a value of 55×10^{-6} cm/s has been obtained for the collective permeability of the two aqueous boundary layers and filter in the unstirred situation (unpublished observation). Therefore, upon rearrangement and substitution we obtain

$$p_{mono} = \frac{1}{\frac{1}{p_{eff}} - \frac{1}{55 \times 10^{-6}}} \quad (2)$$

However, p_{mono} is itself comprised of transcellular and paracellular permeabilities in parallel, i.e.

$$p_{mono} = p_{para} + p_{cell} \quad (3)$$

In general, p_{cell} represents the overall contributions of passive and active transport processes available to a solute. Previous studies with related small-peptide mimetics have demonstrated the presence of a concentration-dependent polarized efflux pathway in Caco-2 cells in addition to the concentration-independent, passive diffusion mechanism.[20,21] As shown in Table 1, the BL → AP effective permeabilities for the *N*-Ac-X-D-Phe-NHMe peptides were greater than AP → BL permeabilities. These differences were eliminated in the presence of 300 μM verapamil in both the donor and receiver chambers, suggesting the involvement of P-glycoprotein in the polarized transport mechanism, similar to the case with a related phenylalanine oligomer series.[21] In contrast, the *N*-Ac-X-phenethylamide peptides showed no polarity in transport or verapamil influences. For the purposes of the present study, we wished to correlate physicochemical properties of the solutes with the passive-diffusional transcellular pathway. Therefore, the effective permeabilities in the presence of verapamil ($p_{eff,verapamil}$), in the case of *N*-Ac-X-D-Phe-NHMe peptides, were employed for further analysis.

Finally, the paracellular permeabilities for the peptides were estimated from a previously established relationship in which paracellular flux is modeled in terms of molecular size-restricted diffusion within an electrostatic field of force.[18,22] Upon substitution of the values into eq 3, p_{cell}, the transcellular passive permeabilities of the peptides, were obtained and are included in Table 1. After application of these corrections Ac-Gly-D-Phe-NHMe and Ac-D-Ala-D-Phe-NHMe are excluded due to their primarily paracellular transport, and Ac-D-Phe-phenethylamide and Ac-D-Cha-phenethylamide (Cha = cyclohexylalanine) are excluded due to their exclusively unstirred water layer-limited diffusion.

In Table 2 are summarized the results of the partition coefficient determinations for the peptide mimetics. Note that within each peptide series the hydrogen-bonding potential, as represented by Δ log *P* (log $P_{n\text{-octanol/water}}$ − log $P_{heptane/water}$), does not vary more than 10%. The average value of Δ log *P* for the X-D-Phe series, with a hydrogen-bond number of 6, is 5.91, whereas for the X-phenethylamide series, with a hydrogen-bond number of 4, the average Δ log *P* value is 4.21.

Table 2. Physicochemical Data for Compounds **1**−**12**

compound	MW	tHB[a]	dHB[a]	aHB[a]	log $P_{octanol/water}$	log $P_{heptane/water}$	Δ log *P*	log $P_{heptane/glycol}$
1	277	6	3	3	0.30	6.30	6.00	6.17
2	291	6	3	3	0.06	6.26	6.20	5.83
3a	319	6	3	3	0.66	5.33	5.99	5.79
4	333	6	3	3	1.24	4.61	5.85	5.43
5a	367	6	3	3	1.44	4.15	5.59	5.34
6	373	6	3	3	2.40	3.41	5.81	5.03
7	220	4	2	2	0.48	3.73	4.21	5.00
8	234	4	2	2	0.76	3.53	4.29	4.40
9a	262	4	2	2	1.59	2.64	4.23	3.77
10	276	4	2	2	2.03	2.14	4.17	3.69
11a	310	4	2	2	2.32	2.00	4.32	3.70
12	316	4	2	2	3.13	0.90	4.03	3.41

[a] tHB = total number of solute hydrogen bonds possible, dHB = number of donor hydrogen bonds, aHB = number of acceptor hydrogen bonds. [b] Standard error for log $P_{octanol/water} \leq 15\%$, for log $P_{heptane/water} \leq 10\%$, for Δ log $P \leq 15\%$, and for log $P_{heptane/ethylene\ glycol} \leq 5\%$; $n \geq 2$ for all solvent partition experiments.

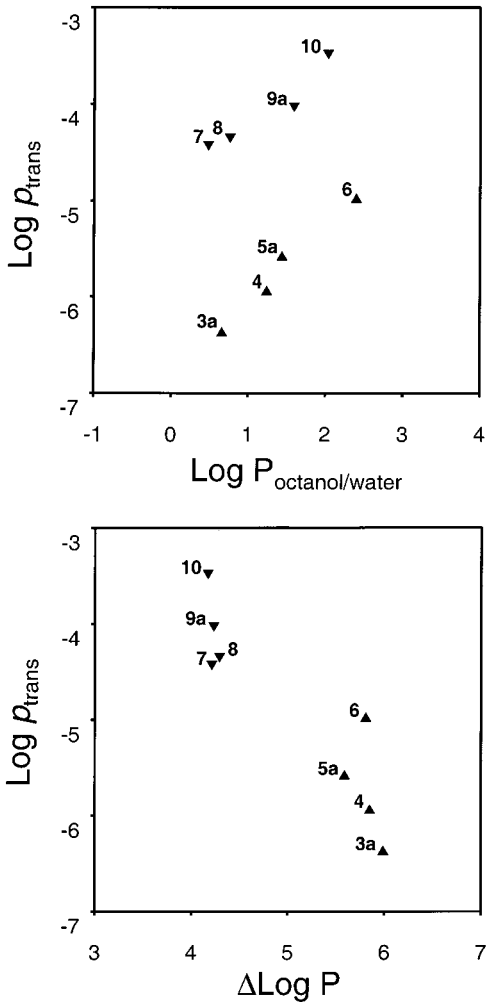

Figure 3. Transcellular permeability for compounds **1**−**12** as a function of (top panel) solute lipophilicity and (bottom panel) solute hydrogen-bond potential; ▲ = *X*-phenylalanine series, ▼ = *X*-phenethylamide series.

Furthermore, the estimated sizes of the peptides, as approximated by their molecular weights, do not vary beyond 10% within each series.

The relationship of transcellular permeability coefficients with octanol−water partition coefficients is shown in Figure 3 (top). Two distinctly different correlations are observed, with the phenethylamide series exhibiting greater cellular permeation than the Phe-

NHMe analogues. Within each series, an incremental increase in permeability is seen with increasing partition coefficient. The corresponding relationship with Δ log *P* is shown in Figure 3 (bottom). Again the solutes form two distinct clusters, with the more permeable solutes having the smaller Δ log *P*. Within each group, differences independent of Δ log *P* are seen in the cellular permeabilities of the individual solutes.

Discussion

One of the most successful conceptual constructs relating drug physicochemical properties with drug absorption is the partition−diffusion model. This posits that the rate of drug transport across an absorbing surface is proportional to the solubility, i.e., partitioning, into the membrane and its diffusion coefficient in the membrane.[23] Implicit in this model is the assumption of homogeneity in the composition of the permeability-limiting membrane. Since membrane partition coefficients are generally difficult to obtain experimentally, surrogate organic solvent partition coefficients are usually employed instead. The most frequently utilized solvent is octanol. Recent work has shown that the solute molecular features important in octanol partitioning are volume and hydrogen-bond basicity.[24] By extrapolation, then, these are assumed to be critical features in drug absorption. For many classes of solutes this seems to be true, and good correlations have been established between drug absorption rates and octanol−buffer partition coefficients.

However, for highly functionalized solutes, such as peptides, this simple relationship does not appear to hold. In this case, partitioning systems that are more dependent upon solute hydrogen-bond donor and acceptor strength, with little or no volume contribution, correlate better with intestinal cellular permeability.[25] Such differences in solute structure−permeability correlations challenge the original assumption of membrane structural homogeneity and suggest the different solutes are experiencing different diffusion-limiting microdomains within the absorbing epithelium. These observations are consistent with earlier studies by Diamond and Katz exploring the validity of the partition/diffusion model for describing the mechanism of solute permeability across phospholipid vesicles.[26] In this case, partition coefficients were determined in dimyristoylphosphatidylcholine (DMPC) vesicles and used to model permeation into those vesicles. In comparing the resulting permeability coefficients with those calculated by assuming the partition diffusion model for a homogeneous membrane, the experimental values were only a small fraction of those expected. The conclusion of these studies was that the rate-limiting barrier to permeation of the solutes was not the region where most of the solute was partitioned but rather a region where the solute was excluded.[26] The simplest inhomogeneous, microdomain model that was consistent with the known structure of phospholipid vesicles consists of a polar, interfacial headgroup region separating the aqueous environment from the much more apolar membrane interior environment where the phospholipid acyl hydrocarbon chains are located. These regions differ in their ability to accommodate hydrogen-bonding groups and/or nonpolar domains on a solute molecule.

This simple model was elaborated in an interesting series of molecular dynamics simulations exploring solute permeation across phospholipid membranes. Marrink and Berendsen[27] proposed a four-compartment model consisting of two interfacial regions differing in hydrogen-bonding characteristics and two interior domains with different free volume distributions. This model was used to define the local resistances to permeation for several solutes with differing hydrogen-bond capacity. For solutes with significant hydrogen-bond potential, association with the interfacial region was favorable but movement into the apolar interior regions presented the most significant barrier. Conversely, solutes with little or no hydrogen-bonding functionality were excluded from the interfacial region but were freely permeable within the membrane interior.[27]

Our results are consistent with these representations of solute membrane microenvironment interactions. We had previously shown that, for a series of phenylalanine oligomers with essentially constant octanol/water partitioning, Caco-2 cell permeability was directly related to the hydrogen-bonding properties of the molecules.[17,25] This supported a model in which such molecules have high affinity for the membrane interfacial region but experience resistance in the interface to interior transfer in which the interfacial hydrogen bonds need to be broken.[25] The energy required for this process could be approximated from the Δ log *P* parameter.

These previous observations have been confirmed and extended in the present study. Comparison of the permeability data for the two series shown in Figure 3 (top) clearly show that cellular permeability is dependent upon hydrogen-bond potential. Compounds **5a** and **9a**, for example, have comparable log $P_{\text{octanol/water}}$ values (1.44 and 1.59, respectively) with a 37-fold difference in permeability. This difference in permeability is consistent with the decrease in the Δ log *P* of approximately 1.7 upon removing the terminal $CONHCH_3$, resulting in two fewer hydrogen-bonding sites in **9a**. Although this structural change is also accompanied by a decrease in molecular size, which could have an impact on the diffusion step, these size changes are relatively modest and are not expected to have much of an impact on the transport of these solutes. Thus these changes are attributed to differences in the free energy of partitioning. Further, given that log $P_{\text{octanol/water}}$ is primarily a measure of volume and hydrogen-bond acceptor strength, the small difference in partition coefficients for **5a** and **9a** suggest that hydrogen-bond basicity contributes little to the observed permeability differences. This indicates that removal of $CONHCH_3$ principally reduces hydrogen-bond donor potential,[28] which is the major factor differentiating permeability for these two solutes.

As shown in Figure 3, within a series of constant Δ log *P*, there is an incremental increase in permeability with octanol−water partition coefficient. Taken altogether, these results further support the presence of different solute−membrane interactions during the permeation process, all of which can influence the overall transport rate. These results can also put into perspective the relative influences of hydrogen-bonding groups and apolar hydrocarbon substituents on the

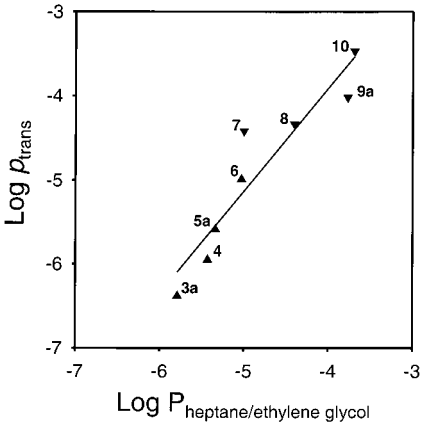

Figure 4. Transcellular permeability versus heptane/ethylene glycol partitioning for compounds **1**−**12**; ▲ = *X*-phenylalanine series, ▼ = *X*-phenethylamide series. The relationship is described by log $p_{cell} = 0.57 \log P_{heptane/ethyleneglycol} - 2.03$, with $r^2 = 0.63$ and $s = 0.49$. Although this supports that both solute volume and hydrogen-bond potential are fundamental determinants of cellular permeability, it is clear that this solvent-partition measure does not accurately represent the interplay of these properties influencing permeability.

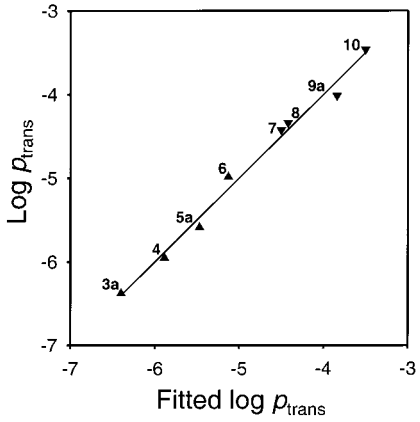

Figure 5. Transcellular permeability as a combined function of solute lipophilicity and hydrogen-bond potential; ▲ = *X*-phenylalanine series, ▼ = *X*-phenethylamide series. The relationship is described by log $p_{cell} = 0.61 \log P_{octanol/water} - 1.13\ \Delta \log P - 0.04$, with $r^2 = 0.99$ and $s = 0.13$. These results suggest that a more specific relationship of solute volume and hydrogen-bond potential, not represented by log $P_{heptane/ethyleneglycol}$, is required in order to describe cellular permeability for these solutes.

permeation process. In the N-Ac-X-D-Phe-NHMe series, as X progresses from hydrogen to cyclohexyl, log $P_{octanol/water}$ increases from −0.3 to 2.4, almost 3 log units, while cellular permeability increases from about 0 to 10.3×10^{-6} cm/s. In contrast, removing hydrogen-bond donor sites, as already discussed in comparing **5a** and **9a**, results in an increase in permeability from 2.6×10^{-6} to 96.4×10^{-6} cm/s. Clearly, removal of hydrogen-bonding functionality is much more effective in improving permeability than introduction of additional hydrocarbon. Such insights may be useful in guiding the design of more bioavailable drug development candidates.

Finally, given that structurally different solutes can experience different permeation limiting interactions within the cell membrane, what is the possibility of establishing a single in vitro model that will predict permeability for a diverse series of solutes? In Figure 4 is shown the relationship of transcellular permeability with log $P_{heptane/glycol}$ for the eight peptide mimetics as a group. Solvatochromic analysis of the log $P_{heptane/glycol}$ system showed that this partition coefficient is reflective of solute hydrogen-bond donor and acceptor potential, similar to the case with Δ log *P*. However, it contains a significant volume contribution, more similar to the situation with log $P_{octanol/water}$.[25,29] Thus it is essentially a hybrid of the two systems. Consistent with these broad property contributions to log $P_{heptane/glycol}$, a better correlation with permeability is obtained than with either log $P_{octanol/water}$ or Δ log *P* alone, systems that are more specific with regard to solute structure. These results contrast with a recent comparison of Δ log *P* and log $P_{heptane/glycol}$ as predictors of cell permeation.[30] In that case, Δ log *P* was found to be more highly correlated with permeation of solutes into algae cells. A possible explanation for this apparent discrepancy may be due to differences in the cell types used in the two studies. Alternatively, the differences in composition of the solutes in the two studies may be sufficient to distinguish their permeability-limiting cell interactions as discussed herein. The present results suggest that a general permeability model for the peptide mimetics examined here will need to incorporate all the solute structural properties important in both log $P_{octanol/water}$ and Δ log *P*.

In support of this proposition is the finding that a weighted, linear combination of log $P_{octanol/water}$ and Δ log *P* gives a reasonably good model for permeability of these solutes (Figure 5). Very similar results were reported recently in modeling efforts with the present data set in the context of a polar surface area (PSA) model.[31] In that report, PSA, which is a putative measure of hydrogen-bond potential for a solute, did not correlate well with the permeability of these solutes, while it had worked well for other, more homologous solutes.[32] However, a reasonably good correlation was obtained by inclusion of a nonpolar surface area term to the model. Although the correlation reported utilized effective permeability coefficients, which are mechanistically complicated as shown in Figure 1, and not transcellular permeability coefficients, the qualitative similarity to our results further supports the conclusion that a general model of permeability will require consideration of a number of solute structural properties.

Experimental Section

Materials and Methods. Caco-2 cells were obtained from the American Type Culture Collections (ATCC), Rockville, MD, at passage 19. All cell culture reagents were from Gibco−BRL, Gaithersburg, MD. Transwells were from Corning Costar, Cambridge, MA. *tert*-Butoxycarbonyl- (BOC-) protected amino acids and verapamil hydrochloride were purchased from Sigma, St. Louis, MO. [^{14}C]Acetic anhydride (105−120 μCi/mmol) was purchased from Amersham. Melting points were obtained on a Hoover Unimelt apparatus and were uncorrected. ^{1}H and ^{13}C NMR spectra were obtained on a Varian 400 spectrometer. Mass spectra and elemental analysis were performed by the Structural and Medicinal Chemistry Group. Reversed-phase high-pressure liquid chromatography (RP-HPLC) was performed on a Hypersil BDS/C_{18} analytical (15 cm × 4.6 mm) column, with a Waters 600 gradient solvent delivery system, a 712 WISP autosampler, and 490 multi-wavelength detector operating at 206 and 254 nm, interfaced

with a 486-based PC running Waters Millenium software for controlling instrumentation and data collection.

Partition Coefficient Determinations. Solvent partition coefficients (*n*-octanol/water, *n*-heptane/water, and heptane/ethylene glycol) were determined as described in detail previously.[17,25] Briefly, a stock solution of the peptide was prepared in the polar phase (water or ethylene glycol) at ca. 5−20 mM (ethylene glycol) or 20 μM (water). Upon dissolution, the stock solution was filtered to remove any undissolved peptide, and aliquots (in triplicate) were placed in clean, oven-dried screw-cap glass vials with Teflon septa. For ethylene glycol/heptane partition experiments, all manipulations of the ethylene glycol stock were done in a low-humidity (<25% relative humidity at 25 °C) room; the water content of the ethylene glycol phase was determined by Karl Fisher titration to be less than 0.2 wt %. HPLC-grade heptane was used in a phase-volume ratio of 100:1 relative to the ethylene glycol solution of peptide. The phases were mixed initially in the sealed screw-cap vials by sonication for 10−15 min and then placed on a wrist-action shaker at 25 °C for at least 2 days to ensure that equilibrium was obtained. The heptane phase (25 mL) was removed with a clean dry glass volumetric pipet and then dried down in vacuo, and the residual peptide was rinsed into an amber silanized glass vial with ca. 1 mL of MeOH. MeOH was removed under a nitrogen stream with warming and the contents were transferred to an HPLC vial with 250 μL of 10% MeOH/water, resulting in a concentration factor of 100. The ethylene glycol phase was diluted with 10% MeOH/water to 30 mL, for a dilution factor of 100. Comparison of the peptide concentrations in the two phases by RP-HPLC, accounting for the concentration and dilution factors, provides the heptane/ethylene glycol partition coefficient as the log of the ratio of the concentrations. For octanol/water partition experiments, the peptide stock solutions were prepared in octanol-saturated water and filtered, and aliquots were placed in screw-cap glass vials in triplicate. Water-saturated octanol was added in a phase-volume ratio of 1:20, and the phases were initially mixed by sonication, followed by agitation on an orbital shaker (200 rpm) for not less than 2 days at room temperature to ensure equilibration. The phases were separated by centrifugation and 300 μL of the aqueous phase was transferred to an HPLC vial for comparison with the initial aqueous peptide stock. The octanol/water partition coefficients were obtained from the log of the ratio of peptide concentrations in the octanol and water phases. The heptane/water partition coefficients were determined in a similar fashion, with a heptane/water phase-volume ratio of 50:1. After 2 days the heptane phase was removed and concentrated and the peptide was taken up into 10% MeOH/water for a concentration factor of 100. Aliquots of the aqueous phase were analyzed, without dilution, by HPLC. The heptane/water partition coefficient was obtained as the log of the ratio of peptide concentrations in the heptane and aqueous phases. For all peptides calibration curves were established to determine the region of linear response of the detector, at 206 nm, to the peptide concentrations.

Cell Culture. Caco-2 cells were cultured as previously described.[14] Briefly, monolayers used in this study were grown at 37 °C with 5% CO_2, in T-150 flasks with Dulbecco's modified Eagle medium (DMEM), pH 7.2, containing 4.5 g/L D-glucose and 584 mg/L L-glutamine, supplemented with 1% (v/v) nonessential amino acids, 1% (v/v) sodium pyruvate, and 10% (v/v) fetal bovine serum. After 1 week the confluent cell monolayers were washed 3× with Hank's balanced salt solution, without calcium or magnesium (HBSS−CMF), and then removed from the flask by incubation with 0.25% (v/v) trypsin in 1 mM EDTA for 10 min at 37 °C. The trypsinized cells were diluted with DMEM/FBS to a concentration of 63 000 cells/cm^2, as determined with a hemocytometer. The Caco-2 cells were seeded into 24-mm-diameter Transwell inserts, with 0.4 μm pore polycarbonate filters, and maintained at 37 °C, 5% CO_2, and 95% relative humidity for at least 14 days prior to use in transport studies. After 7 days the medium was exchanged every second day.

Transport Studies. The procedure for conducting transport studies has been described previously.[14] Briefly, confluent monolayers of between 14 and 21 days, and between passage 25 and 40, were used for transport studies. Prior to use the medium was siphoned off the monolayers, which were then rinsed 3× with phosphate-buffered saline (PBS) containing 15 mM HEPES (pH 7.2) and 0.1% (m/v) D-glucose, and then incubated in PBS/HEPES, 1.5 mL in the apical compartment and 2.5 mL in the basolateral compartment, at 37 °C. For apical-to-basolateral transport experiments, the buffer was removed from the apical (donor) compartment and replaced with 1.5 mL of PBS/HEPES containing [^{14}C]-*N*-acetylated peptide at ca. 250 000 dpm/mL, supplemented with unlabeled peptide to a total peptide concentration of ca. 20 μM. At a specified time interval the monolayer cup was transferred to an adjacent well (receiver compartment) containing fresh buffer. For the basolateral-to-apical transport experiments, the well (donor compartment) was charged with 2.5 mL of the peptide solution and the insert containing the monolayer and buffer (receiver compartment) was then placed in the well. At specified time intervals the buffer in the receiver compartment was removed and replaced with fresh buffer. Time intervals were chosen to maintain sink conditions, such that no greater than 5% of the peptide permeated into the receiver compartment per interval. All experiments were run at 37 °C in a 5% CO_2 atmosphere with 95% relative humidity. Cumulative transport of peptide was obtained by summing the percentage amounts of radionuclide appearing in the receiver compartment after each sampling interval.

Quantitation. Concentrations of the labeled peptides, in disintegrations per minute (dpm) per milliliter, in the receiver solutions were determined by liquid scintillation counting in a Beckman LS 3801 scintillation counter. Effective permeability coefficients (in centimeters per second) were calculated from these concentrations and the following relationship:

$$p_{\mathrm{eff}} = \left[\frac{V_{\mathrm{R}}}{AC_0}\right] \mathrm{d}C/\mathrm{d}t \qquad (4)$$

where V_R is the volume of the receiver compartment, A is the surface area of the monolayer, C_0 is the initial donor concentration, and dC/dt is the slope of the plot of the cumulative receiver concentration with time.

Peptide Synthesis And Purification. All peptides used in this study were prepared by solution-phase methods with diisopropylcarbodiimide (DIC) and hydroxybenzotriazole (HOBT) as the coupling reagents.[33,34]

Preparation of *N*-BOC-D-phenylalanine *N*-Methylamide. An oven-dried round-bottom flask was charged with *N*-BOC-D-phenylalanine *p*-nitrophenyl ester (5.00 g, 12.9 mmol), to which was added $MeCl_2$ (20 mL) under dry nitrogen with stirring. To this solution methylamine (2.0 M in THF, 32 mL, 65.0 mmol, 5.0 equiv) was added via syringe with continued stirring at 0 °C, and immediate generation of a bright yellow color corresponding to the *p*-nitrophenylate anion was observed. The reaction was allowed to warm to room temperature upon removal from the ice bath and monitored by TLC. After 3 h, precipitated methylammonium *p*-nitrophenylate salt was removed by gravity filtration and the solvents were removed in vacuo. The resulting pale yellow solid was triturated with Et_2O/petroleum ether (1:2), and the white microcrystalline solid was collected by vacuum filtration; 3.43 g, 12.3 mmol, 95.3% yield. This material (2.78 g, 10.0 mmol) was then taken up into 8 mL of $MeCl_2$, followed by addition of 7.7 mL of trifluoroacetic acid (TFA, 100 mmol, 10 equiv) with stirring at room temperature. Solvents were removed in vacuo after 1 h and the residue was coevaporated twice with $MeCl_2$, after which the residue was triturated with Et_2O, yielding 2.48 g of the TFA salt of d-phenylalanine *N*-methylamide as a white microcrystalline solid, 8.49 mmol, 85% yield. A further recrystallization of this salt from MeCN provided white microcrystalline needles and removed any residual excess TFA. ^{1}H NMR (400.1 MHz, DMSO-d_6) δ 2.58 (3 H, d, J = 4.4 Hz, NH-CH_3), 2.98 (2 H, m, β-CH_2 (Phe)), 3.90 (1 H, dd, J = 7.2 Hz, α-CH (Phe)), 7.19−7.34 (5 H, m, Ar-H (Phe)), 8.21 (3 H, broad s, CF_3-

CO_2- H_3N^+(Phe)), 8.31 (1 H, d, J = 4.4 Hz, N*H*-CH_3); ^{13}C NMR (100.6 MHz, DMSO-d_6) δ; high-resolution FAB MS m/z 179.1185 ($M^+ + 1$). Anal. Calc. for $C_{12}H_{15}N_2O_3F_3$: C, 49.32; H, 5.17; N, 9.59. Found: C, 49.23; H, 5.06; N, 9.68.

Representative Preparation of *N*-Ac-D-Valine-D-phenylalanine *N*-Methylamide (3). An oven-dried round-bottom flask was charged with *N*-BOC-D-valine (0.22 g, 1.0 mmol), followed by 0.14 g of *dry* 1-hydroxybenzotriazole (HOBT, 1.0 mmol, 1.0 equiv). (Note: 1-hydroxybenzotriazole is commercially available as a hydrate. Dissolution of the hydrate in toluene removes the water as the azeotrope in vacuo, as determined by a Karl Fisher test.) The amino acid and HOBT were suspended in 5 mL of $MeCl_2$, followed by addition of diisopropylcarbodiimide (DIC, 0.16 mL, 1.0 mmol, 1.0 equiv) with stirring under dry nitrogen at 0 °C. After 1 h the TFA salt of D-phenylalanine *N*-methylamide (0.29 g, 1.0 mmol, 1.0 equiv) was added along with 0.14 mL of triethylamine (1.0 mmol, 1.0 equiv), and the reaction was allowed to warm to room-temperature overnight. After 15 h solvents were removed in vacuo and the residue was purified by silica gel flash chromatography ($MeCl_2$/MeOH, 96:4), yielding a white amorphous solid, 0.32 g, 0.84 mmol, 84% yield. The *N*-BOC-protected dipeptide (0.32 g, 0.84 mmol) was dissolved in 4 mL of $MeCl_2$, and to this solution was added TFA (0.65 mL, 8.4 mmol, 10 equiv) with stirring. After 1 h the solvents were removed in vacuo and the residue was triturated with Et_2O, yielding a white granular solid (0.29 g, 0.73 mmol, 87%) recovered by vacuum filtration. The TFA salt of the dipeptide was then resuspended in 4 mL of $MeCl_2$, to which was added acetic anhydride (0.69 mL, 7.3 mmol, 10 equiv) and triethylamine (1.0 mL, 7.3 mmol, 10 equiv) with stirring. After ca. 1 h a precipitate began to form and the solution began to gel. After 15 h the reaction was quenched with ca. 1 mL of MeOH, solvents were removed in vacuo, and the residue was purified by flash chromatography (95:5 $MeCl_2$/MeOH), providing a white solid with some acetic acid still detected by scent. The *N*-acetylated dipeptide was recrystallized from MeOH/water, yielding a white granular solid that was dried in a vacuum desiccator.

The stereomeric purity of the peptides was assessed by comparison of retention times on a chiral HPLC column for the diastereomer pairs *N*-Ac-D-Val/L-Val-D-Phe-NHMe and *N*-Ac-D-Phe/L-Phe-D-Phe-NHMe and for the enantiomeric pairs *N*-Ac-D-Val/L-Val-phenethylamide and *N*-Ac-D-Phe/L-Phe-phenethylamide.

Synthesis and Purification of ^{14}C-Labeled Peptides. The *N*-BOC-protected peptide (50 μmol) to be ^{14}C-labeled was dissolved in $MeCl_2$ (0.5 mL), and trifluoroacetic acid (0.5 mL) was added with stirring at room temperature under an atmosphere of dry nitrogen. After 30 min the solvents were removed in vacuo, and the residue was coevaporated with $MeCl_2$ followed by coevaporation with Et_2O. The free amine was obtained by aqueous workup with $NaHCO_3$ and saturated brine and extracted with $CHCl_3$/MeOH (7:3). After the organic layer was dried over anhydrous Na_2SO_4 and filtered, the solvents were removed in vacuo and the residue was coevaporated twice with $MeCl_2$ to remove residual MeOH. The free amine was dissolved in $MeCl_2$ (2 mL) followed by addition of triethylamine (70 μL, 10 equiv) and bis(2-oxo-3-oxazolidinyl)-phosphinic chloride (BOP-Cl, 2 mg, 0.2 equiv) under dry nitrogen. [1-^{14}C]Acetic anhydride (5% w/w in toluene, 500 μCi) was diluted with 200 μL of $MeCl_2$ under nitrogen, and ca. 250 μCi of the acetic anhydride was transferred to the reaction (the remaining [1-^{14}C]acetic anhydride was used in a separate labeling reaction), which was allowed to proceed overnight at room temperature. Aliquots (ca. 2−5 μL) of the reaction were diluted into 1 mL of 10% aqueous MeOH/MeCN for reversed-phase HPLC analysis with radiolytic detection. In some cases the [^{14}C]acetylated peptide precipitated from solution; redissolution was achieved with addition of 0.5 mL of MeOH. The resultant labeled peptides were stored as the crude product solutions at −40 °C in sealed screw-cap vials. Determination of the specific activity of the solution [in disintegrations per minute (dpm) per microliter] combined with the yield of labeled peptide (relative to total radioactivity) indicated by RP-HPLC provided the volume of crude product solution containing a given quantity (in disintegrations per minute) of labeled peptide. Labeled peptide was purified as needed by preparative silica gel thin-layer chromatography (TLC), using unlabeled peptide to locate the pure peptide band by UV, and recovered from the silica gel by extraction with MeOH/$MeCl_2$ (1:1) and filtration.

Analytical Data. *N*-Acetylglycyl-D-phenylalanine *N*-Methylamide (1). Mp = 195.0−195.5 °C; RP-HPLC retention time (10% MeOH/H_2O:MeCN, 85:15) = 3.0 min; ^{1}H NMR (400.1 MHz, CD_3OD) δ 1.99 (3 H, s, Ac-CH_3), 2.70 (3 H, s, NH-CH_3), 2.91 (1 H, dd, J = 13.6, 8.4 Hz, β-CH_2 (Phe)), 3.15 (1 H, dd, J = 13.6, 8.0 Hz, β-CH_2 (Phe)), 3.78 (2 H, m, J = 16.4 Hz, CH_2 (Gly)), 4.57 (1 H, dd, J = 8.0 Hz, α-C*H* (Phe)), 7.22−7.29 (5 H, m, Ar-*H* (Phe)); ^{13}C NMR (100.6 MHz, CD_3OD) δ 21.5 (Ac-*C*H_3), 25.3 (NH-*C*H_3), 37.8 (β-*C*H_2 (Phe)), 42.6 (*C*H_2 (Gly)), 55.1 (α-*C*H (Phe)), 126.8, 128.5, 129.2, 156.3 (Ar-*C* (Phe)), 170.3 (Ac-*C*O), 171.8 (*C*ONH (Gly)), 172.8 (*C*ONH (Phe)); high-resolution FAB MS m/z 278.1511 ($M^+ + 1$). Anal. Calcd for $C_{14}H_{19}N_3O_3$: C, 60.65; H, 6.86; N, 15.16. Found: C, 60.66; H, 6.81; N, 15.09.

***N*-Acetyl-D-alanyl-D-phenylalanine *N*-Methylamide (2).** Mp = 246.0−247.0 °C; RP-HPLC retention time (10% MeOH/H_2O:MeCN, 85:15) = 3.5 min; ^{1}H NMR (400.1 MHz, DMSO-d_6/10% TFA-d_1) δ 1.00 (3 H, d, J = 6.8 Hz, β-CH_3 (Ala)), 1.81 (3 H, s, Ac-CH_3), 2.55 (3 H, s, NH-CH_3), 2.80 (1 H, dd, J = 13.6, 9.6 Hz, β-CH_2 (Phe)), 3.00 (1 H, dd, J = 13.6, 5.2 Hz, β-CH_2 (Phe)), 4.14 (1 H, q, J = 6.8 Hz, α-C*H* (Ala)), 4.36 (1 H, dd, J = 5.2, 9.6 Hz, α-C*H* (Phe)), 7.15−7.24 (5 H, m, Ar-*H* (Phe)); ^{13}C NMR (100.6 MHz, DMSO-d_6/10% TFA-d_1) δ 18.3 (β-*C*H_3 (Ala)), 23.1 (Ac-*C*H_3), 26.1 (NH-*C*H_3), 38.2 (β-*C*H_2 (Phe)), 49.2 (α-*C*H (Ala)), 54.6 (α-*C*H (Phe)), 127.0, 128.8, 129.9, 138.7 (Ar-*C* (Phe)), 170.3 (Ac-*C*O), 171.8 (*C*ONH (Ala)), 172.8 (*C*ONH (Phe)); high-resolution FAB MS m/z 292.1659 ($M^+ + 1$). Anal. Calcd for $C_{15}H_{21}N_3O_3$: C, 61.86; H, 7.22; N, 14.43. Found: C, 61.82; H, 7.32; N, 13.86.

***N*-Acetyl-D-valyl-D-phenylalanine *N*-Methylamide (3a).** Mp = 274.5−275.0 °C; RP-HPLC retention time (10% MeOH/H_2O:MeCN, 85:15) = 4.2 min; ^{1}H NMR (400.1 MHz, DMF-d_7) δ 0.96 (6 H, 2d, J = 6.8 Hz, γ-CH_3 (Val)), 2.18 (1 H, m, J = 6.8 Hz, β-C*H* (Val)), 2.13 (3 H, s, Ac-CH_3), 2.83 (3 H, d, J = 4.8 Hz, NH-CH_3), 3.10 (1 H, dd, J = 14.0, 9.6 Hz, β-CH_2 (Phe)), 3.31 (1 H, dd, J = 14.0, 5.2 Hz, β-CH_2 (Phe)), 4.29 (1 H, dd, J = 7.6 Hz, α-C*H* (Val)), 4.78 (1 H, ddd, J = 5.2, 8.4, 9.6 Hz, α-C*H* (Phe)), 7.40 (5 H, m, Ar-*H* (Phe)), 7.95 (1 H, m, N*H*-CH_3), 8.21 (1 H, d, J = 8.2 Hz, CON*H* (Val)), 8.26 (1 H, d, J = 8.4 Hz, CON*H* (Phe)); ^{13}C NMR (100.6 MHz, DMF-d_7) δ 18.1 (γ-*C*H_3 (Val)), 19.4 (β-*C*H(Val)), 22.7 (Ac-*C*H_3), 25.9 (NH-*C*H_3), 38.2 (β-*C*H_2 (Phe)), 55.0 (α-*C*H (Val)), 59.8 (α-*C*H (Phe)), 126.8, 128.7, 129.8, 138.9 (Ar-*C* (Phe)), 165.7 (Ac-*C*O), 171.8 (*C*ONH (Val)), 172.1 (*C*ONH (Phe)); high-resolution FAB MS m/z 320.1979 ($M^+ + 1$). Anal. Calcd for $C_{17}H_{25}N_3O_3$: C, 63.93; H, 7.89; N, 13.16. Found: C, 64.03; H, 7.99; N, 12.89.

***N*-Acetyl-D-leucyl-D-phenylalanine *N*-Methylamide (4).** Mp = 223.0−224.0 °C; RP-HPLC retention time (10% MeOH/H_2O:MeCN, 75:25) = 3.1 min; ^{1}H NMR (400.1 MHz, DMSO-d_6/10% TFA-d_1) δ 0.76, 0.81 (6 H, 2d, J = 6.4 Hz, δ-CH_3 (Leu)), 1.30 (2 H, m, β-CH_2 (Leu)), 1.50 (1 H, m, γ-CH (Leu)), 1.81 (3 H, s, Ac-CH_3), 2.54 (3 H, s, NH-CH_3), 2.80 (1 H, dd, J = 13.6, 9.2 Hz, β-CH_2 (Phe)), 2.97 (1 H, dd, J = 13.6, 5.2 Hz, β-CH_2 (Phe)), 4.16 (1 H, dd, J = 6.0, 9.6 Hz, α-C*H* (Leu)), 4.39 (1 H, dd, J = 5.2, 9.2 Hz, α-C*H* (Phe)), 7.14−7.23 (5 H, m, Ar-*H* (Phe)); ^{13}C NMR (100.6 MHz, DMSO-d_6/10% TFA-d_1) δ 22.2, 23.1 (δ-*C*H_3 (Leu)), 23.5 (γ-*C*H(Leu)), 24.8 (Ac-*C*H_3), 26.1 (NH-*C*H_3), 38.2 (β-*C*H_2 (Phe)), 41.1 (β-*C*H_2 (Leu)), 52.1 (α-*C*H (Leu)), 54.5 (α-*C*H (Phe)), 126.9, 128.7, 129.9, 138.6 (Ar-*C* (Phe)), 170.4 (Ac-*C*O), 171.8 (*C*ONH (Leu)), 172.5 (*C*ONH (Phe)); high-resolution FAB MS m/z 334.2129 ($M^+ + 1$). Anal. Calcd for $C_{18}H_{27}N_3O_3$: C, 64.86; H, 8.11; N, 12.61. Found: C, 64.30; H, 8.22; N, 12.58.

***N*-Acetyl-D-phenylalanyl-D-phenylalanine *N*-Methylamide (5a).** Mp = 264.0−265.0 °C; RP-HPLC retention time (10% MeOH/H_2O:MeCN, 75:25) = 3.5 min; ^{1}H NMR (400.1

MHz, DMSO-d_6/30% TFA-d_1) δ 1.85 (3 H, s, Ac-CH_3), 2.62 (3 H, s, NH-CH_3), 2.81 (1 H, dd, J = 14.0, 9.6 Hz, β-CH_2 (Phe)), 2.90 (1 H, dd, J = 13.6, 8.8 Hz, β-CH_2 (Phe)), 3.02 (1 H, dd, J = 14.0, 5.2 Hz, β-CH_2 (Phe)), 3.09 (1 H, dd, J = 13.6, 5.2 Hz, β-CH_2 (Phe)), 4.52 (1 H, dd, J = 5.2, 8.4 Hz, α-C*H* (Phe)), 4.57 (1 H, dd, J = 5.2, 9.2 Hz, α-C*H* (Phe)), 7.08−7.17 (5 H, m, Ar-*H* (Phe)); ^{13}C NMR (100.6 MHz, DMSO-d_6/30% TFA-d_1) δ 22.3 (Ac-*C*H$_3$), 25.7 (NH-*C*H$_3$), 37.8 (β-*C*H$_2$ (Phe)), 38.2 (β-*C*H$_2$ (Phe)), 54.7 (α-*C*H (Phe)), 54.8 (α-*C*H (Phe)), 126.7, 126.8, 128.5, 128.6, 129.7, 129.8, 138.3, 138.4 (Ar-*C* (Phe)), 170.9 (Ac-*C*O), 171.5 (*C*ONH (Phe)), 171.8 (*C*ONH (Phe)); high-resolution FAB MS *m*/*z* 368.1973 ($M^+ + 1$). Anal. Calcd for $C_{21}H_{25}N_3O_3$: C, 68.66; H, 6.81; N, 11.44. Found: C, 68.14; H, 6.99; N, 11.32.

***N*-Acetyl-D-cyclohexylalanyl-D-phenylalanine *N*-Methylamide (6).** Mp = 239.0−240.0 °C; RP-HPLC retention time (10% MeOH/H_2O:MeCN, 65:35) = 3.4 min; ^{1}H NMR (400.1 MHz, DMSO-d_6/30% TFA-d_1) δ 0.68, 0.94, 1.26 (8 H, m, CH_2 (Cha)), 1.43 (5 H, m, γ-C*H*, CH_2 (Cha)), 1.84 (3 H, s, Ac-CH_3), 2.52 (3 H, s, NH-CH_3), 2.76 (1 H, dd, J = 14.0, 8.8 Hz, β-CH_2 (Phe)), 2.95 (1 H, dd, J = 14.0, 5.6 Hz, β-CH_2 (Phe)), 4.20 (1 H, dd, J = 7.2 Hz, α-C*H* (Cha)), 4.51 (1 H, dd, J = 5.6, 8.8 Hz, α-C*H* (Phe)), 6.98−7.08 (5 H, m, Ar-*H* (Phe)); ^{13}C NMR (100.6 MHz, DMSO-d_6/30% TFA-d_1) δ 20.9 (Ac-*C*H$_3$), 25.7 (ϵ-*C*H$_2$ (Cha)), 25.8 (ϵ + 1 *C*H$_2$ (Cha)), 26.0 (NH-*C*H$_3$), 32.1 (γ-*C*H$_2$ (Cha)), 33.2 (δ-*C*H$_2$ (Cha)), 33.8 (β-*C*H$_2$ (Cha)), 38.7 (β-*C*H$_2$ (Phe)), 52.2 (α-*C*H (Cha)), 54.7 (α-*C*H (Phe)), 127.1, 128.6, 129.3, 136.5 (Ar-*C* (Phe)), 173.2 (Ac-*C*O), 173.3 (*C*ONH (Cha)), 174.4 (*C*ONH (Phe)); high-resolution FAB MS *m*/*z* 374.2448 ($M^+ + 1$). Anal. Calcd for $C_{21}H_{31}N_3O_3$: C, 67.53; H, 8.36; N, 11.25. Found: C, 65.95; H, 8.11; N, 10.91.

***N*-Acetylglycine Phenethylamide (7).** Mp = 147.5−148.5 °C; RP-HPLC retention time (10% MeOH/H_2O:MeCN, 80:20) = 3.0 min; ^{1}H NMR (400.1 MHz, DMSO-d_6) δ 1.85 (3 H, s, Ac-CH_3), 2.69 (2 H, d, J = 8.0 Hz, β-CH_2 (phen)), 3.27 (2 H, dt, J = 13.6, 6.0 Hz, α-CH_2 (phen)), 3.61 (2 H, d, J = 5.6, CH_2 (Gly)), 7.19−7.30 (5 H, m, Ar-*H* (phen)), 7.88 (1 H, m, CONH (phen)), 8.04 (1 H, m, CONH (Gly)); ^{13}C NMR (100.6 MHz, DMSO-d_6) δ 24.2 (Ac-*C*H$_3$), 31.8 (β-*C*H$_2$ (phen)), 36.8 (α-*C*H$_2$ (phen)), 43.8 (*C*H$_2$ (Gly)), 127.7, 130.0, 130.3, 141.1 (Ar-*C* (phen)), 170.5 (Ac-*C*O), 171.2 (*C*ONH (Gly)); high-resolution FAB MS *m*/*z* 221.1288 ($M^+ + 1$). Anal. Calcd for $C_{12}H_{16}N_2O_2$: C, 65.45; H, 7.27; N, 12.73. Found: C, 65.51; H, 7.38; N, 12.73.

***N*-Acetyl-D-alanine Phenethylamide (8).** Mp = 151.5−152.5 °C; RP-HPLC retention time (10% MeOH/H_2O:MeCN, 80:20) = 6.1 min; ^{1}H NMR (400.1 MHz, CD_3OD) δ 1.28 (3 H, d, J = 7.2 Hz, β-CH_3 (Ala)), 1.85 (3 H, s, Ac-CH_3), 2.80 (2 H, d, J = 7.2 Hz, β-CH_2 (phen)), 3.39 (2 H, dd, J = 7.2, 8.8 Hz, α-CH_2 (phen)), 4.27 (1 H, q, J = 7.2, CH_2 (Ala)), 7.18−7.31 (5 H, m, Ar-*H* (phen)); ^{13}C NMR (100.6 MHz, CD_3OD) δ 17.1 (β-*C*H$_3$ (Ala)), 21.4 (Ac-*C*H$_3$), 31.8 (β-*C*H$_2$ (phen)), 40.9 (α-*C*H$_2$ (phen)), 49.5 (α-*C*H$_2$ (Ala)), 126.3, 128.4, 128.9, 139.4 (Ar-*C* (phen)), 172.0 (Ac-*C*O), 174.1 (*C*ONH (Ala)); high-resolution FAB MS *m*/*z* 235.1450 ($M^+ + 1$). Anal. Calcd for $C_{13}H_{18}N_2O_2$: C, 66.67; H, 7.69; N, 11.97. Found: C, 66.42; H, 7.61; N, 11.73.

***N*-Acetyl-D-valine Phenethylamide (9a).** Mp = 219.5−220.5 °C; RP-HPLC retention time (10% MeOH/H_2O:MeCN, 80:20) = 9.0 min; ^{1}H NMR (400.1 MHz, DMSO-d_6/10% TFA-d_1) δ 0.83 (6 H, d, J = 6.8 Hz, γ-CH_3 (Val)), 1.95 (3 H, s, Ac-CH_3), 1.97 (1 H, m, β-C*H* (Val)), 2.75 (2 H, t, J = 6.8 Hz, β-CH_2 (phen)), 3.30, 3.40 (2 H, m, α-CH_2 (phen)), 4.12 (1 H, d, J = 6.8 Hz, CH_2 (Val)), 7.11−7.24 (5 H, m, Ar-*H* (phen)); ^{13}C NMR (100.6 MHz, DMSO-d_6/10% TFA-d_1) δ 18.1, 19.6 (γ-*C*H$_3$ (Val)), 22.7 (Ac-*C*H$_3$), 31.2 (β-*C*H (Val)), 36.1(β-*C*H$_2$ (phen)), 41.1 (α-*C*H$_2$ (phen)), 59.0 (α-*C*H (Val)), 126.7, 128.9, 129.4, 140.3 (Ar-*C* (phen)), 170.1 (Ac-*C*O), 171.9 (*C*ONH (Val)); high-resolution FAB MS *m*/*z* 263.1758 ($M^+ + 1$). Anal. Calcd for $C_{15}H_{22}N_2O_2$: C, 68.70; H, 8.40; N, 10.69. Found: C, 67.97; H, 8.55; N, 10.54.

***N*-Acetyl-D-leucine Phenethylamide (10).** Mp = 133.0−134.0 °C; RP-HPLC retention time (10% MeOH/H_2O:MeCN, 70:30) = 5.2 min; ^{1}H NMR (400.1 MHz, DMF-d_7) δ 0.85, 0.88 (6 H, 2d, J = 6.8, 6.4 Hz, δ-CH_3 (Val)), 1.50 (2 H, m, β-CH_2 (Leu)), 1.62 (1 H, m, J = 6.4 Hz, γ-C*H* (Leu)), 1.93 (3 H, s, Ac-CH_3), 2.76 (2 H, dd, J = 7.2 Hz, β-CH_2 (phen)), 3.39 (2 H, m, α-CH_2 (phen)), 4.38 (1 H, m, J = 8.8 Hz, α-C*H* (Leu)), 7.20−7.32 (5 H, m, Ar-*H* (phen)), 7.86 (1 H, d, J = 8.0 Hz, CONH (Leu)), 7.95 (1 H, m, CONH (phen)); ^{13}C NMR (100.6 MHz, DMF-d_7) δ 21.6 (γ-*C*H$_3$ (Leu)), 22.5 (Ac-*C*H$_3$), 25.0 (γ-*C*H (Leu)), 35.9 (β-*C*H$_2$ (phen)), 41.0 (α-*C*H$_2$ (phen)), 41.8 (β-*C*H$_2$ (Leu)), 52.0 (α-*C*H (Leu)), 126.5, 128.7, 129.2, 140.2 (Ar-*C* (phen)), 169.8 (Ac-*C*O), 172.8 (*C*ONH (Leu)); high-resolution FAB MS *m*/*z* 277.1918 ($M^+ + 1$). Anal. Calcd for $C_{16}H_{24}N_2O_2$: C, 69.57; H, 8.70; N, 10.14. Found: C, 68.30; H, 8.32; N, 9.82.

***N*-Acetyl-D-phenylalanine Phenethylamide (11a).** Mp = 171.5−172.5 °C; RP-HPLC retention time (10% MeOH/H_2O:MeCN, 60:40) = 6.8 min; ^{1}H NMR (400.1 MHz, DMSO-d_6/10% TFA-d_1) δ 1.85 (3 H, s, Ac-CH_3), 2.73 (2 H, dd, J = 6.0 Hz, β-CH_2 (phen)), 2.77 (1 H, dd, J = 9.2, 14.0 Hz, β-CH_2 (Phe)), 2.98 (1 H, dd, J = 5.2, 14.0 Hz, β-CH_2 (Phe)), 3.35 (2 H, m, α-CH_2 (phen)), 4.51 (1 H, dd, J = 5.2, 9.2 Hz, α-C*H* (Phe)), 7.11−7.20 (5 H, m, Ar-*H* (phen)); ^{13}C NMR (100.6 MHz, DMSO-d_6/10% TFA-d_1) δ 22.5 (Ac-*C*H$_3$), 35.7 (β-*C*H$_2$ (phen)), 38.4 (β-*C*H$_2$ (Phe)), 40.7 (α-*C*H$_2$ (phen)), 54.9 (α-*C*H (Phe)), 126.6, 126.8, 128.6, 128.8, 129.2, 129.8, 138.6, 140.1 (Ar-*C* (Phe, phen)), 170.5 (Ac-*C*O), 171.7 (*C*ONH (Phe)); high-resolution FAB MS *m*/*z* ($M^+ + 1$). Anal. Calcd for $C_{16}H_{24}N_2O_2$: C, 73.79; H, 6.80; N, 9.06. Found: C, 71.16; H, 7.01; N, 8.77.

***N*-Acetyl-D-cyclohexylalanine Phenethylamide (12).** Mp = 131.0−132.0 °C; RP-HPLC retention time (10% MeOH/H_2O:MeCN, 60:40) = 5.4 min; ^{1}H NMR (400.1 MHz, DMSO-d_6) δ 0.84 (2 H, m, ϵ-CH_2 (Cha)), 1.11 (4 H, m, δ-CH_2 (Cha)), 1.35 (2 H, m, β-CH_2 (Cha)), 1.61 (5 H, m, γ-CH_2, α-C*H* (Cha)), 1.81 (3 H, s, Ac-CH_3), 2.68 (2 H, dd, J = 7.2 Hz, β-CH_2 (phen)), 3.24 (2 H, m, J = 7.6 Hz, α-CH_2 (phen)), 4.22 (1 H, m, J = 5.2 Hz, α-C*H* (Cha)), 7.18−7.28 (5 H, m, Ar-*H* (phen)), 7.88 (1 H, d, J = 8.4 Hz, CONH (Cha)), 7.92 (1 H, m, CONH (phen)); ^{13}C NMR (100.6 MHz, DMSO-d_6) δ 23.4(Ac-*C*H$_3$), 26.4, 26.5, 26.9, 32.8, 33.9, 34.3 (ring *C*H, *C*H$_2$ (Cha)), 35.9 (β-*C*H$_2$ (phen)), 41 (β-*C*H$_2$ (Cha)), 41 (α-*C*H$_2$ (phen)), 51.1 (α-*C*H (Cha)), 126.9, 129.1, 129.5, 140.2 (Ar-*C* (Phe, phen)), 169.8 (Ac-*C*O), 172.9 (*C*ONH (Cha)); high-resolution FAB MS *m*/*z* 317.2235 ($M^+ + 1$). Anal. Calcd for $C_{19}H_{28}N_2O_2$: C, 72.15; H, 8.86; N, 8.86. Found: C, 72.11; H, 8.81; N, 9.00.

***N*-Acetyl-L-valyl-D-phenylalanine *N*-Methylamide (3b).** Mp = 265.5−266.5 °C; RP HPLC retention time (Dynamax C-18, 0.46 × 25 cm; 1.0 mL/min; H_2O:MeCN, 75:25; detected at 206 nm) = 9.1 min (compared with the D,D-diastereomer U-98001, retention time = 6.7 min); ^{1}H NMR (400.1 MHz, DMSO-d_6) δ 0.47, 0.61 (6 H, 2d, J = 6.4, 6.8 Hz, γ-CH_3 (Val)), 1.66 (1 H, m, J = 6.8 Hz, β-C*H* (Val)), 1.84 (3 H, s, Ac-CH_3), 2.58 (3 H, d, J = 4.8 Hz, NH-CH_3), 2.69 (1 H, dd, J = 11.2, 13.6 Hz, β-CH_2 (Phe)), 3.08 (1 H, dd, J = 4.0, 13.6 Hz, β-CH_2 (Phe)), 3.91 (1 H, dd, J = 7.6 Hz, α-C*H* (Val)), 4.41 (1 H, m, α-C*H* (Phe)), 7.14−7.22 (5 H, m, Ar-*H* (Phe)), 7.86 (1 H, m, N*H*-CH$_3$), 7.89 (1 H, d, J = 7.2 Hz, CON*H* (Val)), 8.32 (1 H, d, J = 8.4 Hz, CON*H* (Phe)); ^{13}C NMR (100.6 MHz, DMSO-d_6) δ 19.2, 19.7 (γ-*C*H$_3$ (Val)), 23.2 (β-*C*H(Val)), 26.5 (Ac-*C*H$_3$), 30.5 (NH-*C*H$_3$), 38.1 (β-*C*H$_2$ (Phe)), 55.1 (α-*C*H (Val)), 60.0 (α-*C*H (Phe)), 127.0, 128.8, 129.9, 139.0 (Ar-*C* (Phe)), 170.7 (Ac-*C*O), 172.1 (*C*ONH (Val)), 172.2 (*C*ONH (Phe)); high-resolution FAB MS *m*/*z* 320.1982 ($M^+ + 1$). Anal. Calcd for $C_{17}H_{25}N_3O_3$: C, 63.93; H, 7.89; N, 13.16. Found: C, 63.49; H, 7.85; N, 12.99.

***N*-Acetyl-L-valine Phenethylamide (9b).** Mp = 218.0−219.0 °C; RP HPLC retention time (Chiralcel OD-H, 0.46 × 25 cm; 0.5 mL/min; 2-propanol:hexane, 5:95; detected at 206 nm) = 16.1 min (compared with the D-enantiomer U-145144, retention time = 12.9 min); ^{1}H NMR (400.1 MHz, DMSO-d_6) δ 0.76, 0.78 (6 H, 2 d, J = 2.0 Hz, γ-CH_3 (Val)), 1.85 (3 H, s, Ac-CH_3), 1.87 (1 H, m, J = 6.8 Hz, β-C*H* (Val)), 2.70 (2 H, dd, J = 7.2 Hz, β-CH_2 (phen)), 3.22, 3.30 (2 H, m, α-CH_2 (phen)), 4.05 (1 H, d, J = 7.2 Hz, CH_2 (Val)), 7.16−7.28 (5 H, m, Ar-*H* (phen)); ^{13}C NMR (100.6 MHz, DMSO-d_6) δ 19.0, 20.0 (γ-*C*H$_3$ (Val)), 23.3 (Ac-*C*H$_3$), 31.1 (β-*C*H (Val)), 35.9 (β-*C*H$_2$ (phen)), 40.2 (buried under DMSO peak; α-*C*H$_2$ (phen)), 58.7 (α-*C*H (Val)), 126.9, 129.1, 129.5, 140.2 (Ar-*C* (phen)), 170.0 (Ac-*C*O), 171.8 (*C*ONH (Val)); high-resolution FAB MS *m*/*z* 263.1754 ($M^+ + 1$). Anal. Calcd for $C_{15}H_{22}N_2O_2$: C, 68.67; H, 8.45; N, 10.68. Found: C, 68.06; H, 8.42; N, 10.51.

***N*-Acetyl-L-phenylalanyl-D-phenylalanine *N*-Methylamide (5b).** Mp = 247.0−248.0 °C; RP HPLC retention time (Dynamax C-18, 0.46 × 25 cm; 1.0 mL/min; H_2O:MeCN, 75:25; detected at 206 nm) = 17.4 min (compared with the D,D-diastereomer U-97995, retention time = 12.9 min); ^{1}H NMR (400.1 MHz, DMSO-d_6) δ 1.72 (3 H, s, Ac-CH_3), 2.43 (1 H, dd, J = 13.6 Hz, β-CH_2 (Phe)), 2.58 (3 H, s, NH-CH_3), 2.60 (1 H, dd, β-CH_2 (Phe)), 2.71 (1 H, dd, J = 13.6, 10.0 Hz, β-CH_2 (Phe)), 2.97 (1 H, dd, J = 13.6 Hz, β-CH_2 (Phe)), 4.43 (2 H, m, α-C*H* (Phe)), 7.06−7.23 (10 H, m, Ar-*H* (Phe)), 7.91 (1 H, d, J = 3.0 Hz, N*H*CH$_3$), 7.97 (1 H, d, J = 8.0 Hz, CON*H* (Phe)), 8.38 (1 H, d, J = 8.4 Hz, CON*H* (Phe)); ^{13}C NMR (100.6 MHz, DMSO-d_6) δ 23.2 (Ac-*C*H$_3$), 26.4 (NH-*C*H$_3$), 38.3 (β-*C*H$_2$ (Phe)), 38.6 (β-*C*H$_2$ (Phe)), 54.8 (α-*C*H (Phe)), 55.0 (α-*C*H (Phe)), 127.0, 127.1, 128.7, 128.8, 129.9, 130.0, 138.7, 138.8 (Ar-*C* (Phe)), 170.1 (Ac-*C*O), 172.0 (*C*ONH (Phe)), 172.1 (*C*ONH (Phe)); high-resolution FAB MS m/z 368.1973 ($M^+ + 1$). Anal. Calcd for $C_{21}H_{25}N_3O_3$: C, 68.64; H, 6.86; N, 11.44. Found: C, 67.44; H, 6.66; N, 11.16.

***N*-Acetyl-L-phenylalanine Phenethylamide (11b).** Mp = 170.5−171.5 °C; RP HPLC retention time (Chirobiotic, 0.5 mL/min; MeOH:H_2O, 30:70; detected at 206 nm) = 18.0 min (compared with the D-enantiomer U-145147, retention time = 21.2 min).

^{1}H NMR (400.1 MHz, DMSO-d_6) δ 1.75 (3 H, s, Ac-CH_3), 2.65 (2 H, dd, J = 7.2 Hz, β-CH_2 (phen)), 2.68 (1 H, dd, J = 9.6, 13.6 Hz, β-CH_2 (Phe)), 2.88 (1 H, dd, J = 4.8, 13.6 Hz, β-CH_2 (Phe)), 3.23 (2 H, m, α-CH_2 (phen)), 4.41 (1 H, dd, J = 4.8 Hz, α-C*H* (Phe)), 7.16−7.29 (5 H, m, Ar-*H* (phen)), 8.06 (2 H, m, CON*H* (Phe, phen); ^{13}C NMR (100.6 MHz, DMSO-d_6) δ 23.3 (Ac-*C*H$_3$), 35.9 (β-*C*H$_2$ (phen)), 38.7 (β-*C*H$_2$ (Phe)), 40.7 (α-*C*H$_2$ (phen), buried under DMSO peak), 54.9 (α-*C*H (Phe)), 126.9, 127.0, 128.8, 129.1, 129.5, 129.9, 138.9, 140.2 (Ar-*C* (Phe, phen)), 169.8 (Ac-*C*O), 171.9 (*C*ONH (Phe)); high-resolution FAB MS m/z 311.1761 ($M^+ + 1$). Anal. Calcd for $C_{16}H_{24}N_2O_2$: C, 73.52; H, 7.14; N, 9.02. Found: C, 72.47; H, 7.02; N, 8.90.

Acknowledgment. We thank Allen R. Hilgers and Alan Clarke for assisting with performance of the permeability studies and partition coefficient determinations. We also acknowledge Dr. Boryeu Mao from Computer Aided Drug Discovery and Dr. Thomas J. Vidmar (Biostatistics) for helpful discussions.

References

(1) Pond, S. M.; Tozer, T. N. First-pass elimination. Basic concepts and clinical consequences. *Clin. Pharmacokinet.* **1984**, *9*, 1−25.
(2) Navia, M. A.; Chaturvedi, P. R. Design principles for orally bioavailable drugs. *Drug Discovery Today* **1996**, *1*, 179−189.
(3) Mayerson, M. Principles of drug absorption. In *Modern Pharmaceutics*, 2nd ed.; Banker, G. S., Rhodes, C. T., Eds.; Marcel Dekker: New York, 1990; pp 23−90.
(4) Trier, J. S. Structure of the mucosa of the small intestine as it relates to intestinal function. *Fed. Proc.* **1967**, *26*, 1391−1404.
(5) Parson, D. S.; Boyd, C. A. R. Transport across the intestinal mucosal cell: hierarchies of function. *Int. Rev. Cytol.* **1972**, *32*, 209−255.
(6) Crissinger, K. D.; Kvietys, P. R.; Granger, D. N. Pathophysiology of gastrointestinal mucosal permeability. *J. Int. Med.* **1990**, *228* (Suppl. 1), 145−154.
(7) Wright, E. M. Solute and water transport across epithelia. *Am. Rev. Respir. Dis.* **1983**, *127*, S3−S8.
(8) Diamond, J. M. The epithelial junction: bridge, gate and fence. *Physiologist* **1977**, *20*, 10−18.
(9) Gumbiner, B. Structure, biochemistry and assembly of epithelial tight junctions. *Am. J. Physiol.* **1987**, *253*, C749−58.
(10) Conradi, R. A.; Hilgers, A. R.; Ho, N. F. H.; Burton, P. S. The influence of peptide structure on transport across Caco-2 cells. *Pharm. Res.* **1991**, *8*, 1453−1460.
(11) Conradi, R. A.; Hilgers, A. R.; Ho, N. F. H.; Burton, P. S. The influence of peptide structure on transport across Caco-2 cells. II. Peptide bond modification which results in improved permeability. *Pharm. Res.* **1992**, *9*, 435−439.
(12) Pinto, M.; Robine-Leon, S.; Appay, M. D.; Kedinger, M.; Triadou, N.; Dussaulx, E.; LaCroix, B.; Simon-Assman, P.; Haffen, K.; Fogh, J.; Zweibaum, A. Enterocyte-like differentiation and polarization of the human colon carcinoma cell line Caco-2 in culture. *Biol. Cell* **1983**, *47*, 323−330.
(13) Hidalgo, I. J.; Raub, T. J.; Borchardt, R. T. Characterization of the human colon carcinoma cell line (Caco-2) as a model system for intestinal epithelial permeability. *Gastroenterology* **1989**, *96*, 736−749.
(14) Hilgers, A. R.; Conradi, R. A.; Burton, P. S. Caco-2 cell monolayers as a model for drug transport across the intestinal mucosa. *Pharm. Res.* **1990**, *7*, 902−910.
(15) Artursson, P. Epithelial transport of drugs in cell culture. I: a model for studying the passive diffusion of drugs over intestinal absorptive (Caco-2) cells. *J. Pharm. Sci.* **1990**, *79*, 476−482.
(16) Wilson, G.; Hassan, I. F.; Dix, C. J.; Williamson, I.; Shah, R.; Mackay, M.; Artursson, P. Transport and permeability properties of human Caco-2 cells: an in vitro model of the intestinal epithelial cell barrier. *J. Controlled Release* **1990**, *11*, 25−40.
(17) Burton, P. S.; Conradi, R. A.; Hilgers, A. R.; Ho, N. F. H.; Maggiora, L. L. The relationship between peptide structure and transport across epithelial cell monolayers. *J. Controlled Release* **1992**, *19*, 87−98.
(18) Adson, A.; Burton, P. S.; Raub, T. J.; Barsuhn, C. L.; Hilgers, A. R.; Audus, K. L.; Ho, N. F. H. Passive diffusion of weak organic electrolytes across Caco-2 cell monolayers: uncoupling the contributions of hydrodynamics, transcellular and paracellular barriers. *J. Pharm. Sci.* **1995**, *84*, 1197−1204.
(19) Ho, N. F. H.; Raub, T. J.; Burton, P. S.; Barsuhn, C. L.; Adson, A.; Audus, K. L.; Borchardt, R. T. Quantitative Approaches to Delineate Transport Mechanisms in Cell Culture Monolayers. In *Transport Processes in Pharmaceutical Systems*; Himmelstein, K. J., Amidon, G. L., Lee, P. I., Eds.; Marcel Dekker: New York, 1999; pp 219−316.
(20) Burton, P. S.; Conradi, R. A.; Hilgers, A. R.; Ho, N. F. H. Evidence for a polarized efflux system for peptides in the apical membrane of Caco-2 cells. *Biochem. Biophys. Acta* **1993**, *190*, 760−766.
(21) Burton, P. S.; Goodwin, J. T.; Conradi, R. A.; Ho, N. F. H.; Hilgers, A. R. In vitro permeability of peptidomimetic drugs: the role of polarized efflux pathways as additional barriers to absorption. *Adv. Drug Deliv. Rev.* **1997**, *23*, 143−156.
(22) Adson, A.; Raub, T. J.; Burton, P. S.; Barsuhn, C. L.; Hilgers, A. R.; Audus, K. L.; Ho, N. F. H. Quantitative approaches to delineate paracellular diffusion in cultured epithelial cell monolayers. *J. Pharm. Sci.* **1994**, *83*, 1529−1536.
(23) Schanker, L. S. On the mechanism of absorption of drugs from the gastrointestinal tract. *J. Med. Pharm. Chem.* **1960**, *2*, 343−359.
(24) El Tayer, N.; Tsai, R.-S.; Testa, B.; Carrupt, P.-A.; Leo, A. Partitioning of solutes in different solvent systems: the contribution of hydrogen-bonding capacity and polarity. *J. Pharm. Sci.* **1991**, *80*, 590−598.
(25) Paterson, D. W.; Conradi, R. A.; Hilgers, A. R.; Vidmar, T. J.; Burton, P. S. A nonaqueous system for predicting the oral absorption potential of peptides. *Quant. Struct.-Act. Relat.* **1994**, *13*, 4−10.
(26) Diamond, J. M.; Katz, Y. Interpretation of nonelectrolyte partition coefficients between dimyristoyl lecithin and water. *J. Membr. Biol.* **1975**, *17*, 121−154.
(27) Marrink, S. J.; Berendsen, H. J. C. Permeation process of small molecules across lipid membranes studied by molecular dynamics simulations. *J. Phys. Chem.* **1996**, *100*, 16729−16738.
(28) Leo, A. J. Evaluating hydrogen-bond donor strength. *J. Pharm. Sci.* **2000**, *89*, 1567−1578.
(29) Abraham, M. H.; Martins, F.; Mitchell, R. C.; Salter, C. J. Hydrogen bonding. 47. Characterization of the ethylene glycol−heptane partition system: hydrogen bond acidity and basicity of peptides. *J. Pharm. Sci.* **1999**, *88*, 241−247.
(30) Platts, J. A.,; Abraham, M. J.; Hersey, A.; Butina, D. Estimation of molecular linear free energy relationship descriptors. 4. Correlation and predicition of cell permeation. *Pharm. Res.* **2000**, *17*, 1013−1018.
(31) Stenberg, P.; Luthman, K.; Artursson, P. Prediction of membrane permeability to peptides from calculated molecular surface properties. *Pharm. Res.* **1999**, *16*, 205−212.
(32) Palm, K.; Luthman, K.; Ungell, A.-L.; Strandlund, G.; Artursson, P. Correlation of drug absorption with molecular surface properties. *J. Pharm. Sci.* **1996**, *85*, 32−39.
(33) Tartar, A.; Gesquiere, J. C. Formation of CH_2Cl_2-soluble urea derivatives during solid-phase peptide synthesis with unsymmetrical carbodiimides. *J. Org. Chem.* **1979**, *44*, 5000−5002.
(34) Beyermann, M.; Henklein, P.; Klose, A.; Sohr, R.; Bienert, M. Effect of tertiary amine on the carbodiimide-mediated peptide synthesis. *Int. J. Pept. Protein Res.* **1991**, *37*, 252−256.

JM010253I